Electron-positron pair production in frequency modulated laser fields

C. Gong,[1] Z. L. Li,[1,2,*] B. S. Xie,[3,4,†] and Y. J. Li[1,‡]

[1]*State Key Laboratory for GeoMechanics and Deep Underground Engineering, China University of Mining and Technology, Beijing 100083, China*
[2]*School of Science, China University of Mining and Technology, Beijing 100083, China*
[3]*Key Laboratory of Beam Technology of the Ministry of Education, and College of Nuclear Science and Technology, Beijing Normal University, Beijing 100875, China*
[4]*Beijing Radiation Center, Beijing 100875, China*

(Received 25 July 2019; revised manuscript received 13 December 2019; published 8 January 2020)

The momentum spectrum and the number density of created electron-positron pairs in a frequency modulated laser field are investigated using the quantum kinetic equation. It is found that the momentum spectrum presents an obvious interference pattern. This is an imprint of the frequency modulated field on the momentum spectrum, because the momentum peaks correspond to the pair production process by absorbing different frequency component photons. Moreover, the interference effect can also be understood qualitatively by analyzing turning-point structures. The study of the pair number density shows that the number density is very sensitive to modulation parameters and can be enhanced by 2 or 3 orders of magnitude for certain modulation parameters, which may provide a new way to increase the number of created electron-positron pairs in future experiments.

DOI: 10.1103/PhysRevD.101.016008

I. INTRODUCTION

Since Dirac predicted the existence of the positron [1], Sauter found that the vacuum could be broken into electron-positron pairs in a very strong static electric field [2], and then Schwinger pointed out that producing observable pairs the field strength should reach the critical field strength $E_{\mathrm{cr}} \approx 10^{18}$ V/m by calculating the pair creation rate in a constant electric field with the proper time method [3]. In order to study how energy is converted into mass, many methods have been proposed [4,5], such as the world-line instanton [6,7], computation quantum field theory [8–11], Wentzel-Kramers-Brillouin (WKB) approximation [12–14], and quantum kinetic method [15–19].

However, the current laser intensity $\sim 10^{22}$ W/cm^2 is still much smaller than the laser intensity corresponding to the critical field strength $\sim 10^{29}$ W/cm^2. Therefore, it is impossible to produce observable electron-positron pairs experimentally only by the Schwinger tunneling mechanism. Moreover, another mechanism that is called multiphoton pair production can also break the vacuum into electron-positron pairs by absorbing several high-energy photons [20,21]. Unfortunately, current laser facilities cannot provide high enough energetic photons for creating observable pairs from vacuum as well. To overcome this limitation, several catalytic mechanisms are put forward to create observable electron-position pairs in subcritical conditions. For example, the dynamically assisted Schwinger mechanism [17,22,23] can significantly enhance pair production by effectively combining the above two pair creation mechanisms. Another way to enhance the number of created pairs is the use of frequency chirped fields [24–27]. It shows that the number density of created particles can be improved several orders of magnitude for suitable chirp parameters. However, it should be noted that in previous works the chirp parameter is not limited. Thus the pair creation can be greatly enhanced by absorbing photons with an extremely high frequency component of the chirped field. Moreover, the momentum distribution of created particles is very sensitive to the chirp parameter, so one can only give a qualitative understanding of the momentum spectrum instead of a quantitative one.

In this paper, we study the details about electron-positron pair creation in a sinusoidal frequency modulated electric field by solving the quantum Vlasov equation (QVE) numerically. This type of field can also be seen as a sinusoidal frequency chirped electric field. By giving a relatively reasonable restriction on modulation parameters, it is found that the number density of created pairs can still be enhanced by 2 or 3 orders of magnitude for certain modulation parameters. Moreover, the interference pattern on the momentum spectrum is an imprint of the information carried by the modulated field and can be quantitatively understood by bridging momentum peaks and the frequency spectrum of the frequency modulated field. And a

*zlli@cumtb.edu.cn
†bsxie@bnu.edu.cn
‡lyj@aphy.iphy.ac.cn

qualitative understanding of the interference effect is also given by analyzing turning-point structures. In addition, the momentum and the number of created pairs can be artificially controlled by adjusting the modulation parameters of the frequency modulated electric field. By the way, this frequency modulated field may be also a good choice to check if the Dirac vacuum can transmit the information carried by this modulated field [28].

This paper is organized as follows: In Sec. II we briefly introduce the method of the QVE, which permits us to calculate the momentum distribution and the number density of created particles. In Sec. III, we analyze the momentum spectrum within a semiclassical method, and we also study the relationship between the momentum peak and the laser frequency component of the frequency modulated field. Moreover, we consider the number density of created particles for different modulation parameters. Section IV is a summary about this work.

II. THE QUANTUM VLASOV EQUATION AND THE EXTERNAL FIELD

The background laser field we used is a spatially homogeneous but time-dependent electric field $\mathbf{E}(t) = (0, 0, E(t))$, and the corresponding vector potential is $\mathbf{A}(t) = (0, 0, A(t))$ with $E(t) = -\dot{A}(t)$. Starting from the Dirac equation in the above field, one can derive the quantum Vlasov equation satisfied by the one-particle momentum distribution function $f(\mathbf{p}, t)$ by a canonical time-dependent Bogoliubov transformation,

$$\frac{df(\mathbf{p},t)}{dt} = \frac{1}{2}\frac{eE(t)\varepsilon_\perp}{\Omega^2(\mathbf{p},t)}\int_{t_0}^{t} dt' \frac{eE(t')\varepsilon_\perp}{\Omega^2(\mathbf{p},t')}[1-2f(\mathbf{p},t')] \times \cos\left[2\int_{t'}^{t} d\tau\Omega(\mathbf{p},\tau)\right], \quad (1)$$

where $-e$ and m denotes the electron charge and mass, respectively. $\mathbf{p} = (\mathbf{p}_\perp, p_\parallel)$ is the canonical momentum, and $\varepsilon_\perp^2 = m^2 + \mathbf{p}_\perp^2$ represents the square of the perpendicular energy, $\Omega^2(\mathbf{p}, t) = \varepsilon_\perp^2 + k_\parallel^2(t)$ is the square of total energy, and $k_\parallel(t) = p_\parallel - eA(t)$ is the kinetic momentum along the direction of the electric field $E(t)$. In this paper, the natural unit $\hbar = c = 1$ is used. Also note that the one-particle distribution function $f(\mathbf{p}, t)$ is only a description of the generated real particles at $t \to +\infty$ where the external electric field is 0. Thus, we are just interested in the distribution function $f(\mathbf{p}, \infty)$ and the particle number density $n(\infty)$.

To solve Eq. (1) numerically, one can introduce two auxiliary variables $u(\mathbf{p}, t) = \int_{t_0}^{t} dt' W(\mathbf{p}, t')[1 - 2f(\mathbf{p}, t')] \times \cos[2\Theta(\mathbf{p}, t', t)]$ and $v(\mathbf{p}, t) = \int_{t_0}^{t} dt' W(\mathbf{p}, t')[1 - 2f(\mathbf{p}, t')] \times \sin[2\Theta(\mathbf{p}, t', t)]$. Then Eq. (1) can be equivalently transformed into the following first-order ordinary differential equations,

$$\begin{aligned}
\frac{df(\mathbf{p},t)}{dt} &= \frac{1}{2}W(\mathbf{p},t)u(\mathbf{p},t),\\
\frac{du(\mathbf{p},t)}{dt} &= W(\mathbf{p},t)[1-2f(\mathbf{p},t)] - 2\Omega(\mathbf{p},t)v(\mathbf{p},t),\\
\frac{dv(\mathbf{p},t)}{dt} &= 2\Omega(\mathbf{p},t)u(\mathbf{p},t),
\end{aligned} \quad (2)$$

where $W(\mathbf{p}, t) = eE(t)\varepsilon_\perp/\Omega^2(\mathbf{p}, t)$ and $\Theta(\mathbf{p}, t', t) = \int_{t'}^{t} d\tau\Omega(\mathbf{p}, \tau)$.

Finally, the single particle distribution function $f(\mathbf{p}, t)$ can be obtained by solving Eqs. (2) with the initial conditions $f(\mathbf{p}, -\infty) = u(\mathbf{p}, -\infty) = v(\mathbf{p}, -\infty) = 0$. Then, the number density of created particles per $d^2p_\perp/(2\pi)^2$ evolving over time reads

$$n(t) = 2\int \frac{dp_\parallel}{2\pi} f(p_\parallel, t), \quad (3)$$

where the factor 2 comes from the degeneracy of electrons.

In this paper, the configuration of the frequency modulated electric field [29] is

$$E(t) = E_0 e^{-\frac{t^2}{2\tau^2}} \cos(\omega t + b\sin(\omega_m t)), \quad (4)$$

where E_0, ω, and τ are the strength, the frequency, and the pulse duration of the electric field, respectively, ω_m is called modulated frequency and b is a parameter that measures the degree of modulation.

To help explain the following numerical results, we depict some typical Fourier transform of the field Eq. (4) in Figs. 1 and 2. In Fig. 1(a), the modulation parameters are $\omega_m = 0.07m$ and $b = 1$, and some frequency components are labeled as $\omega_0 \sim \omega_4$. If we choose $\omega_m = 0.1m$, then the

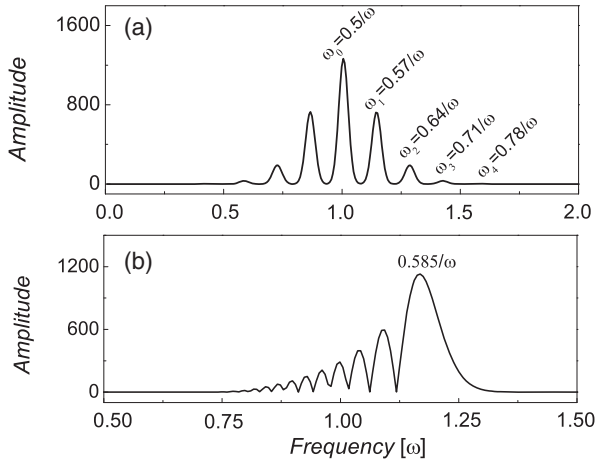

FIG. 1. The Fourier transform of the frequency modulated electric field Eq. (4) with modulation parameters (a) $\omega_m = 0.07m$, $b = 1.0$ and (b) $\omega_m = 0.01m$, $b = 9.52$. Some typical values of frequency peaks are labeled on both panels. Other field parameters are $E_0 = 0.1E_{\rm cr}$, $\omega = 0.5m$, and $\tau = 100/m$.

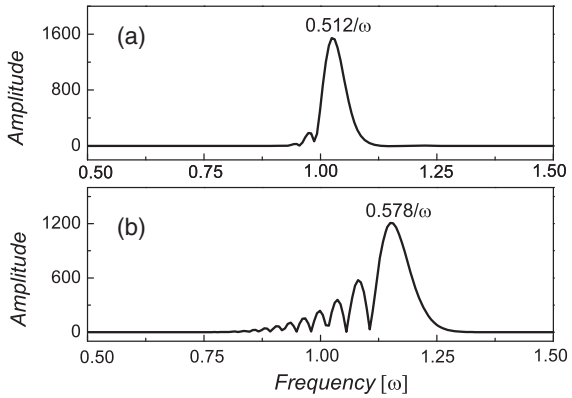

FIG. 2. The Fourier transform of the frequency modulated electric field, where the values of modulation parameter (ω_m, b) are (0.01, 1.52) for the upper panel and (0.009, 9.52) for the lower panel. And the values of dominant frequency peaks are shown. Other field parameters are $E_0 = 0.1E_{\rm cr}$, $\tau = 100/m$, $\omega = 0.5m$.

frequency components that are larger than the original frequency are $\omega_5 = 0.6m$, $\omega_6 = 0.7m$, $\omega_7 = 0.8m$, and $\omega_8 = 0.9m$. For a large degree of modulation, the frequency spectrum is shown in Fig. 1(b), where the modulation parameters are $\omega_m = 0.01m$ and $b = 9.52$. One can see that the original frequency is not the main frequency anymore. This feature can also be seen in Fig. 2.

III. NUMERICAL SIMULATIONS

In this section, we show and analyze the momentum spectra and number density of created electron-positron pairs in the frequency modulated electric field.

A. Theoretical framework based on turning-point structures

In order to clearly understand the interference effects of momentum spectra and the number density of created electron-positron pairs shown in Secs. III B and III C, we first give the theoretical framework in this subsection. That is the phase-integral method [30–32]. The pair creation from vacuum in a spatially homogeneous and time-dependent modulated electric field is similar to the one-dimensional over-the-barrier scattering problem in quantum mechanics, and the momentum distribution function of created pairs can be obtained by the reflection coefficient.

$$f(\mathbf{p}) \approx \sum_{t_p} e^{-2K^p_{\mathbf{p}}} + \sum_{t_p \neq t_{p'}} 2\cos(2\theta^{(p,p')}_{\mathbf{p}})(-1)^{p-p'} e^{-K^p_{\mathbf{p}}-K^{p'}_{\mathbf{p}}}, \tag{5}$$

with

$$K^p_{\mathbf{p}} = \left| \int_{t^*_p}^{t_p} \Omega(\mathbf{p}, t) dt \right|, \quad \theta^{(p,p')}_{\mathbf{p}} = \left| \int_{\mathrm{Re}(t_p)}^{\mathrm{Re}(t_{p'})} \Omega(\mathbf{p}, t) dt \right|,$$

where t_p and $t_{p'}$ represent different turning points, which are the solutions of equation $\Omega(\mathbf{p}, t) = 0$. It is not hard to see that $K^p_{\mathbf{p}}$ and $\theta^{(p,p')}_{\mathbf{p}}$ determine the created pair's number and the degree of interference, respectively. To be specific, the particle number is dominated by the turning points that are nearest to the real time axis, while the degree of interference depends on the pair number of these turning points that are nearest to the real time axis. Therefore, the distribution of turning points on the complex time axis can be used to analyze the information of momentum spectra qualitatively, especially some specific momentum peaks.

Note that, when the electric field is modulated, the analytic expression for turning points cannot be derived, so we give the distribution of these turning points by solving equation $\Omega(\mathbf{p}, t) = 0$ numerically; see the turning point structures shown in Fig. 3.

B. Momentum spectrum

Generally, there are two different mechanisms that can induce electron-positron pair creation from vacuum. One is the Schwinger effect (tunneling mechanism) and the other one is the multiphoton absorption. These two mechanisms can be well distinguished by the adiabaticity parameter $\gamma = m\omega/|e|E_0$ [33]. For the former one $\gamma \ll 1$ and for the latter one $\gamma \gg 1$. Whereas, in this paper we are focused on the interesting intermediate regime $\gamma \sim \mathcal{O}(1)$. For instance, the adiabaticity parameter $\gamma = 5$ for the modulated field with $E_0 = 0.1E_{\rm cr}$ and $\omega = 0.5m$.

Figure 4 shows the momentum spectrum of created particles in frequency modulated fields with different modulation parameters. It can be seen that the momentum spectra in the modulated field have an obvious interference pattern and the interference effect becomes more and more obvious with the increase of the modulation frequency. This result can be understood qualitatively by the theoretical framework given in the above subsection. For the sake of illustration, we show the peak positions of the momentum spectra labeled as 1, 2 ,..., and 19 on Fig. 4 in Table I. In the framework of the phase-integral method, we know that the momentum spectrum shows a Gaussian-like shape when only one pair of turning points dominates the pair production process, while it presents an obvious oscillation structure when more than one pair of turning points dominates. So we think that the interference effects shown in Fig. 4 correspond to the domination of multiple pairs of turning points on pair creation. To see this clearly, we depict several turning-point structures in Fig. 3.

From Fig. 3(a) to Fig. 3(f), the distribution of turning points corresponds to the momentum value p_1, p_5, p_{11}, p_{16}, p_{17}, and p_{18} in Fig. 4, respectively. For the first row in Fig. 3, the modulation frequency ω_m is 0, $0.07m$ and $0.1m$ from left to right, respectively. We find that as the modulation frequency increases the periodicity of these turning points becomes shorter and shorter, and there will be more pair numbers of turning points close to the real

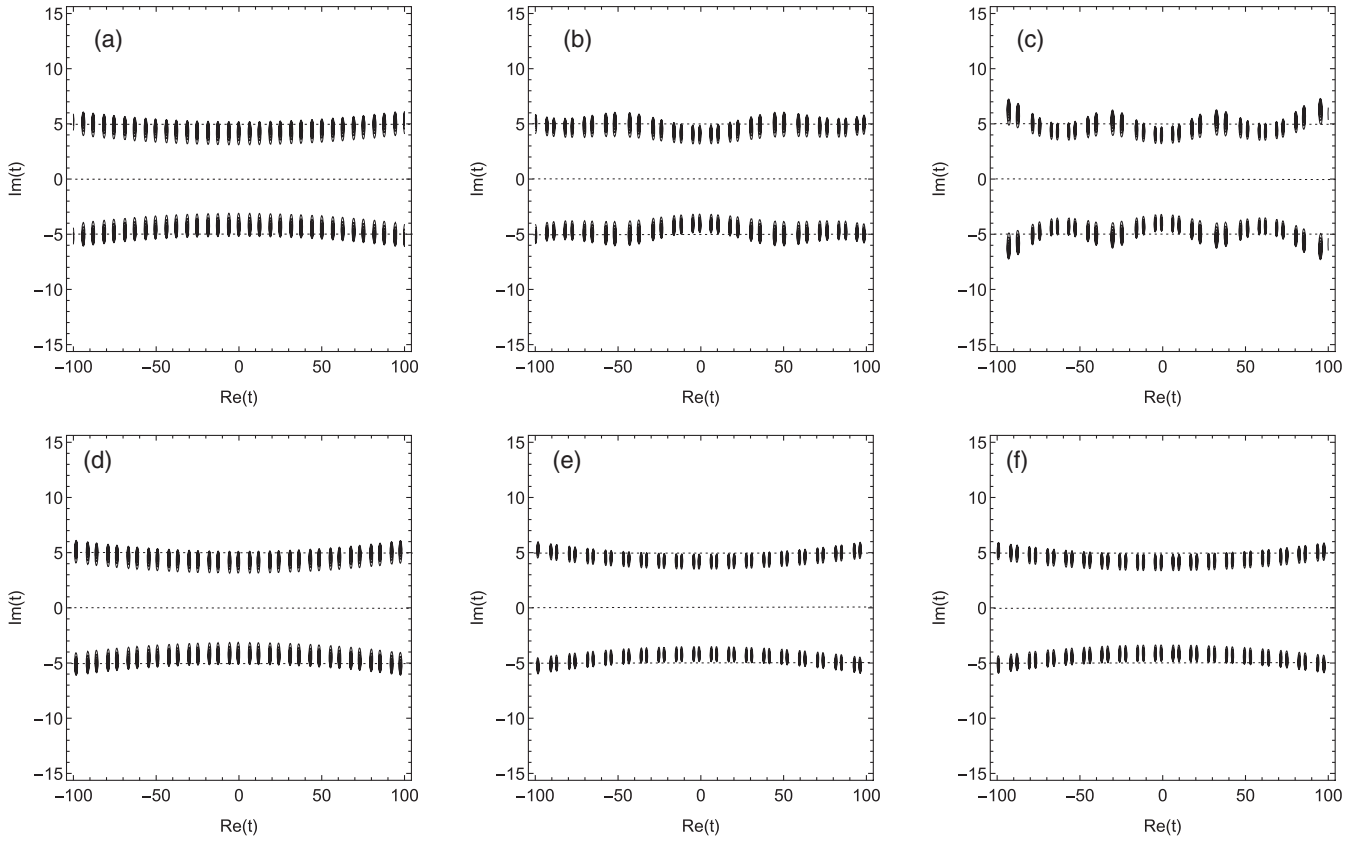

FIG. 3. Contour plots of $|\Omega(\mathbf{p},t)|^2$ in the complex t plane, showing the location of turning points where $\Omega(\mathbf{p},t)=0$. For the upper three panels from left to right the modulation frequency and momentum correspond to $\omega_m=0$, $p_1=0.08m$; $\omega_m=0.07m$, $p_5=0.356m$; $\omega_m=0.1m$, $p_{11}=0.44m$, respectively, and $b=1.0$. For the lower three panels from left to right the momentum values are p_{16}, p_{17}, and p_{18}, respectively. The modulation parameters are the same as in Figs. 2(a), 1(b), and 2(b), respectively. Other field parameters are $E_0=0.1E_{\mathrm{cr}}$, $\omega=0.5m$, and $\tau=100/m$.

time axis. Thus, the interference effect of the momentum spectrum becomes more and more obvious; see the first row in Fig. 4. Furthermore, due to the fact that the turning points in Fig. 3(c) are closer to the real axis than that in Fig. 3(a), the magnitude of momentum peak p_{11} in Fig. 4(c) is smaller than that of p_1 in Fig. 4(a). Of course, the magnitude of other momentum peaks can also be qualitatively analyzed by comparing the distance of turning points to the real time axis. And for Figs. 3(d)–3(f) with the modulation frequency $\omega_m=0.01m$, $0.01m$, and $0.009m$, respectively, one can see that the period of turning points is not obvious, because the period of turning points depends on the modulation frequency and the modulation frequency in Figs. 3(d)–3(f) is much less than that in Figs. 3(b) and 3(c). Comparing the pair number of turning points nearest the real time axis between Figs. 3(e) and 3(f) and Fig. 3(a), we can also find that the inference effect is more obvious for the former two figures than the latter one. Additionally, since the turning points in Fig. 3(e) are farther from the real axis than that in Fig. 3(d), the magnitude of momentum peaks in Fig. 4(d) where $b=1.52$ is significantly larger than that in Fig. 4(e) where $b=9.52$. And we elaborate further on the specific reasons that affect the number of created particles in the next subsection.

In the following, we provide an understanding of this interference effect more quantitatively and physically. According to the definition of total energy of a created electron, the total energy of created electron-positron pairs is

$$E(\mathbf{p})=2\sqrt{m_*^2+\mathbf{p}^2}, \tag{6}$$

where $m_*=m\sqrt{1+\frac{e^2}{m^2}\frac{E_0^2}{2\omega^2}}$ is called effective mass [34]. So the total energy $E_1, E_2, \ldots$, and E_{19} that corresponds to the momentum peak $p_1, p_2, \ldots$, and p_{19} can be calculated by the above equation. For example, in Fig. 4(a), we can obtain the total energy $E_1=2.02$ and $E_2=2.49$ according to Eq. (6). Furthermore, we find that $E_1\approx 4\omega_0$ and $E_2\approx 5\omega_0$, so according to the energy conservation the created particles with momentum p_1 and p_2 correspond to four- and five-photon absorption process, respectively. And the number of created particles by four-photon absorption is much greater than that by five-photon absorption.

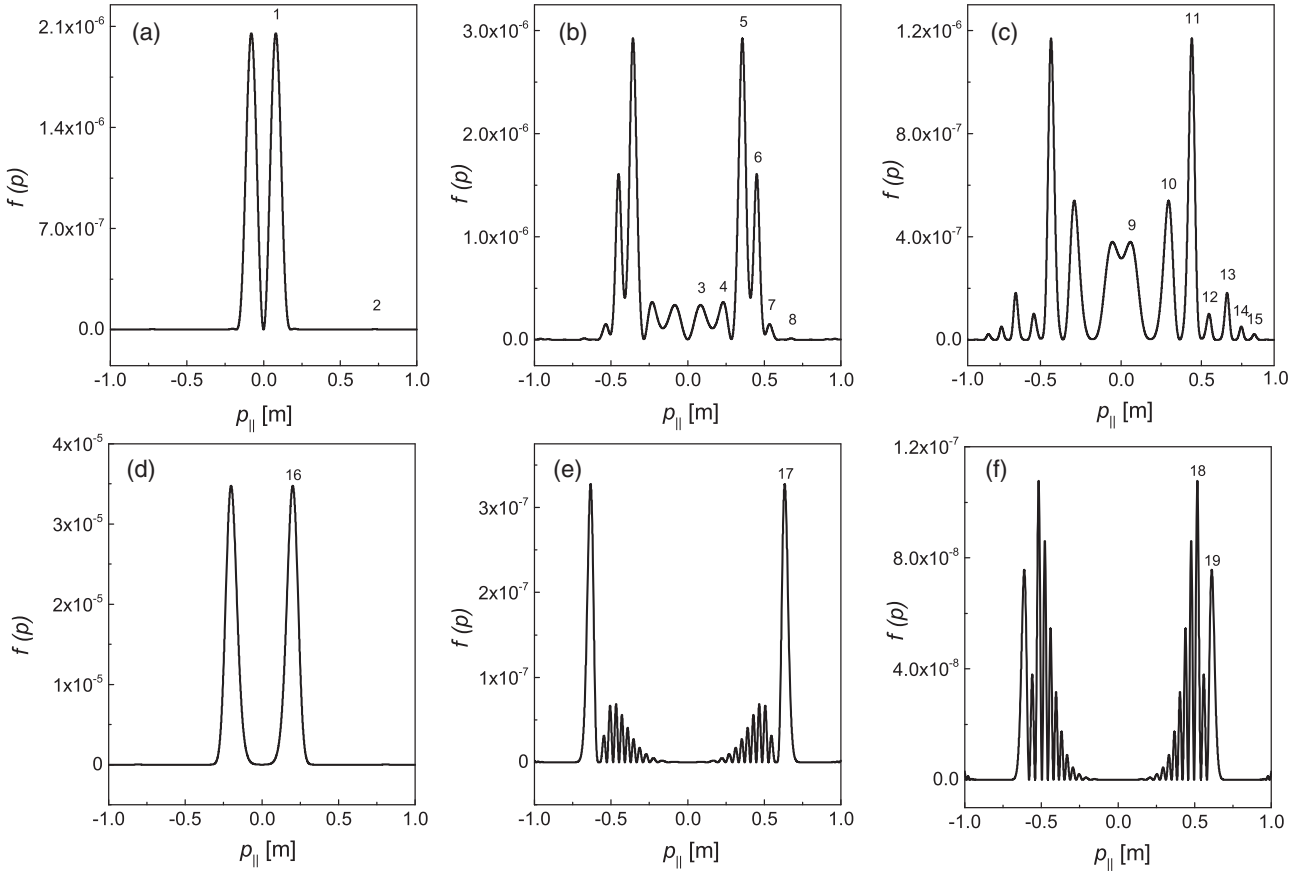

FIG. 4. The momentum spectra of created pairs in the modulated electric field with different modulation parameters. The modulation frequencies for (a)–(c) are $\omega_m = 0.00, 0.07m$ and $0.10m$, respectively. The degree of modulation is $b = 1.0$. The modulation parameters (ω_m, b) for (d)–(f) are (0.01, 1.52), (0.01, 9.52), and (0.009, 9.52), respectively. Other field parameters are $E_0 = 0.1E_{\rm cr}$, $\omega = 0.5m$, and $\tau = 100/m$.

For Figs. 4(b) and 4(c), the modulation frequency ω_m is $0.07m$ and $0.1m$, respectively. Because of the fact that E_3, $E_9 \approx 2.02 \approx 4\omega_0$ and E_8, $E_{14} \approx 2.50 = 5\omega_0$, the created pairs with momentum p_3 and p_9 correspond to four-photon absorption and the created particles with momentum p_8 and p_{14} correspond to five-photon absorption process. In addition to these momentum peaks corresponding to four- and five-photon absorption, one can also see that there are other momentum peaks in Figs. 4(b) and 4(c). For Fig. 4(b) where the modulation frequency $\omega_m = 0.07m$, the total energy of created pairs $E_4 \sim E_7$ corresponding to momentum peaks $p_4 \sim p_7$ is 2.07, 2.14, 2.21, and 2.28, respectively. Based on energy conservation, these momentum peaks are still caused by the four-photon absorption process, because $E_4 \approx 3\omega_0 + \omega_1$, $E_5 \approx 3\omega_0 + \omega_2$, $E_6 \approx 3\omega_0 + \omega_3$, and $E_7 \approx 3\omega_0 + \omega_4$. By the way, since the original frequency dominates the frequency components of the modulated electric field, a large number of photons with frequency ω_0 are absorbed in pair creation. Similar to the above discussions, for Fig. 4(c) with the modulation frequency $\omega_m = 0.1m$, the total energy of created pairs $E_{10} \sim E_{13}$ corresponding to momentum peaks $p_{10} \sim p_{13}$ is 2.10, 2.20, 2.29, and 2.41, and $E_{10} \approx 3\omega_0 + \omega_5$, $E_{11} \approx 3\omega_0 + \omega_6$, $E_{12} \approx 3\omega_0 + \omega_7$, $E_{13} \approx 3\omega_0 + \omega_8$. So these momentum peaks also correspond to four-photon absorption process. Moreover, the total energy E_{15} corresponding to the momentum peak p_{15} is 2.61. This peak is caused by a five-photon absorption process, because $E_{15} \approx 4\omega_0 + \omega_6$.

For the momentum spectrum of created pairs in a modulated field with a large degree of modulation b, see Figs. 4(d)–4(f); the momentum peaks can also be determined by the frequency spectrum of the modulated

TABLE I. The momentum values p_n (n from 0 to 19) of Fig. 4. The unit is m.

p_1	p_2	p_3	p_4	p_5	p_6	p_7	p_8	p_9	p_{10}	p_{11}	p_{12}	p_{13}	p_{14}	p_{15}	p_{16}	p_{17}	p_{18}	p_{19}
0.080	0.728	0.083	0.232	0.356	0.451	0.535	0.731	0.059	0.294	0.440	0.547	0.658	0.746	0.828	0.196	0.633	0.517	0.611

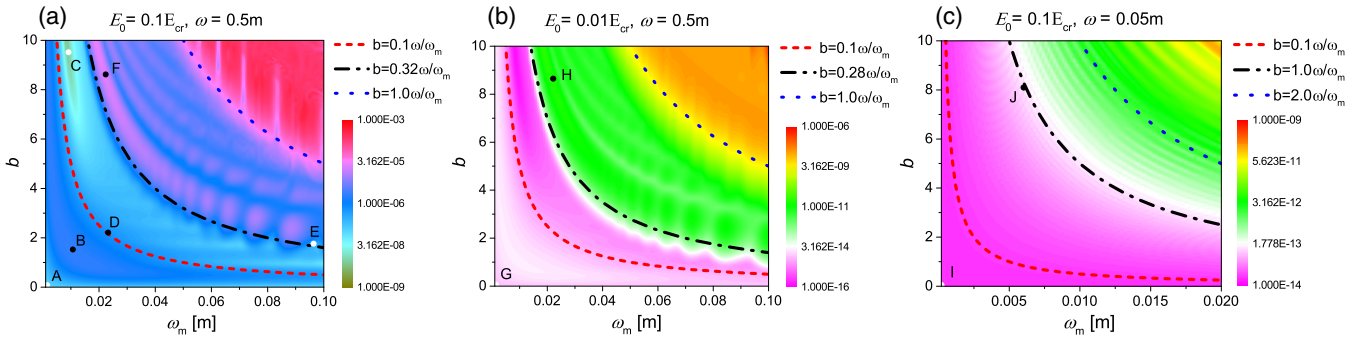

FIG. 5. The number of the created e^-e^+ pairs under the modulated electric field. The red short dash, black dash dot, and blue dot line are the dividing line between the degree of frequency modulation. The white points A, C, E, G, I, K represent the zone-minimum values for each region, while the black points B, D, F, H, J, L represent the zone-maximum values. From left to right, the electric field strength $E_0 = 0.1E_{\rm cr}$, $0.01E_{\rm cr}$, and $0.1E_{\rm cr}$, respectively, and the laser frequency $\omega = 0.5m$, $0.5m$, and $0.05m$, respectively. The other parameters $\tau = 100/m$, b and ω_m are variables.

field. For instance, according to Eq. (6), we have $E_{16} = 2.05 \approx 4 \times 0.512$, $E_{17} = 2.38 \approx 4 \times 0.585$, $E_{18} = 2.26 \approx 3 \times 0.578 + 0.52$, and $E_{19} = 2.35 \approx 4 \times 0.578$, where 0.512, 0.585, and 0.578 are exactly the dominant frequency components [see Figs. 2(a), 1(b), and 2(b)], and 0.52 is the frequency component corresponding to the third highest peak in Fig. 2(b). Thus the momentum peaks p_{16}, p_{17}, p_{18}, and p_{19} also correspond to a four-photon absorption process. Moreover, we are surprised to find that the number of created pairs for p_{18} is larger than that for p_{19}, though the momentum peak p_{19} corresponds to the pair production by absorbing four photons with the dominant frequency component of the modulated electric field. This phenomenon can also be seen in Figs. 4(b) and 4(c), where the highest momentum peak does not always correspond to the pair creation by absorbing four original frequency photons, though the original frequency dominates the frequency components. This finding is explained in Sec. III C.

Based on the analysis of turning-point structures and the momentum peaks, we have a clear physical picture about how the interference effect came about. On one hand, we can use a frequency modulated laser beam to create electron-positron pairs with a predictable and particular momentum by suitable modulation parameters. On the other hand, the frequency components of a frequency modulated field can be well achieved by analyzing the momentum peaks, because the interference pattern is a direct imprint of the frequency modulated field on momentum spectra.

C. Pair number density

In this subsection, we study the number density of the created electron-positron pairs in frequency modulated electric fields. To keep the modulation within a reasonable range, we rewrite the modulated field (4) as

$$E(t) = E_0 e^{-\frac{t^2}{2\tau^2}} \cos(\omega_{\rm eff} t), \tag{7}$$

where $\omega_{\rm eff} = \omega + \frac{b\sin(\omega_m t)}{t}$ is a time-dependent effective frequency, and set $|\frac{b\sin(\omega_m t)}{t}| \le \alpha\omega$ with $0 \le \alpha < 1$ for any time t. Because of $|\frac{b\sin(\omega_m t)}{t}|_{\rm max} = b\omega_m$, we further obtain $b\omega_m \le \alpha\omega$. Finally we have the constraint relation between the degree of modulation b and the modulation frequency ω_m as

$$b \le \frac{\alpha\omega}{\omega_m}. \tag{8}$$

To help study the effect of modulation parameters on the number density of created electron-positron pairs, we draw several typical curves (the red dashed, black dash-dot, and blue dotted lines) according to Eq. (8) on Fig. 5, which shows the pair number density created in the frequency modulated electric field with different modulation parameters. The electric field strength and frequency in Figs. 5(a)–5(c) are $(0.1E_{\rm cr}, 0.5m)$, $(0.01E_{\rm cr}, 0.5m)$, and $(0.1E_{\rm cr}, 0.05m)$, respectively. The degree of modulation b varies from 0 to 10, and the modulation frequency ω_m is chosen to ensure $\omega_m \ll \omega$. According to the red dashed line, i.e., $\alpha = 0.1$, for any frequency modulated electric field with modulation parameters below the parameters of the red dashed line, the maximum value of the effective frequency of the modulated electric field is no more than $\omega + 0.1\omega$, which has the same order of magnitude as the laser frequency ω without modulation. Because of the same reason, for the black dash-dot line where $\alpha = 0.32$ in Fig. 5(a), we can see that the number density of created particles divided by the black dash-dot line has an obvious change. It has the same change for the blue dotted line where $\alpha = 1.0$ in Fig. 5(a).

From Fig. 5, one can see that the number density of created pairs in several different areas that are separated by the typical lines has obvious minimum and maximum values. The minimum values are marked by white points A, C, E, G, I and the maximum values are marked with black points B, D, F, H, J. The modulation parameters (ω_m, b)

TABLE II. The number density for different selected sets of modulation constants (ω_m, b); see the points marked in Fig. 5.

(ω_m, b)	Number density
$A(0, 0)$	1.04×10^{-7}
$B(0.01, 1.52)$	2.00×10^{-6}
$C(0.009, 9.52)$	7.63×10^{-9}
$D(0.023, 2.24)$	6.10×10^{-7}
$E(0.096, 0.96)$	9.89×10^{-8}
$F(0.022, 8.64)$	2.03×10^{-5}
$G(0, 0)$	8.61×10^{-15}
$H(0.022, 8.64)$	2.05×10^{-11}
$I(0, 0)$	1.79×10^{-14}
$J(0.006, 8.10)$	1.58×10^{-13}

and the number density of created pairs corresponding to each minimum and maximum values are shown in Table II. The result in the case of without frequency modulation, i.e., $\omega_m = b = 0$, is also given.

For Fig. 5(a) where the laser frequency $\omega = 0.5m$, when the laser frequency is not modulated, the number density of created particles is 1.04×10^{-7}. Whereas for $0 \leq \alpha \leq 0.1$, the range of modulation parameters (ω_m, b) is below the red dashed line, and the minimum and maximum values of the pair number density in this region are A: 1.04×10^{-7} and B: 2.00×10^{-6}, respectively. It is found that the number density of created pairs corresponding to point B is 20 times greater than that without frequency modulation. For $0.1 \leq \alpha \leq 0.32$, the range of modulation parameters is between the black dash-dot line and the red dashed line, and the minimum and maximum values of the particle number density in this region are C: 7.63×10^{-9} and D: 6.1×10^{-7}, respectively. Although the maximum value of the number density corresponding to point D is larger than that without frequency modulation, it is smaller than that corresponding to point B where the modulation parameters belong to $0 \leq \alpha \leq 0.1$. Moreover, the number density of created particles corresponding to point C is even smaller than that without frequency modulation. This amazing result is caused by the same reason as the phenomenon occurring in Fig. 4, where the highest momentum peak does not always correspond to pair creation by absorbing the photons with dominant frequency component. To explain this result, we give the number density of created pairs varying with the field frequency; see Fig. 6. It can be seen that the pair number density is very sensitive to the field frequency. For example, the number density of created pairs by absorbing four photons with $\omega = 0.512m$ is at least an order of magnitude greater than the one by absorbing four photons with $\omega = 0.5m$. By analyzing the frequency spectra of the frequency modulated field at point B (upper panel) and point C (lower panel) shown in Fig. 2, we find that the dominant frequency components at point B and C are $0.512m$ and $0.578m$, which correspond to a peak and a valley of the particle

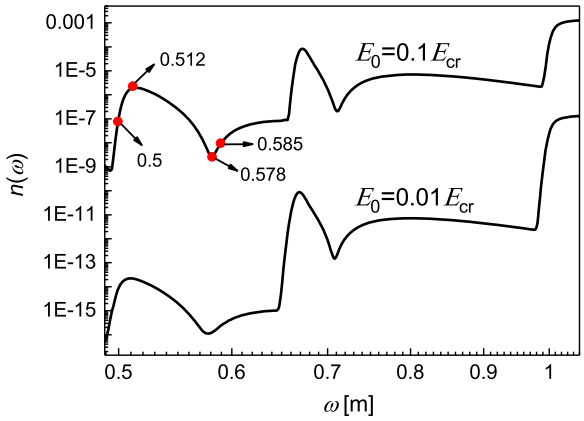

FIG. 6. The number density of created electron-positron pairs as a function of field frequency ω. The oscillating structures are related to the n-photon thresholds. The upper line corresponds to $E_0 = 0.1E_{cr}$ and the lower line corresponds to $E_0 = 0.01E_{cr}$. Other field parameters are $\tau = 100/m$. Note that there is no frequency modulation, i.e., $b = 0$.

number density shown in Fig. 6, respectively. Therefore, the pair number density at point B is larger than the one without frequency modulation ($\omega = 0.5m$), while the number density at point C is smaller than the latter one. A similar result can also be found by comparing the values of momentum peaks in Figs. 4(d), 4(a), and 4(f). Moreover, we know that the momentum peak p_{18} in Fig. 4(f) is formed by absorbing three photons with $\omega = 0.578$ and one photon with $\omega = 0.52$, and the number density for $\omega = 0.52$ is much larger than that for $\omega = 0.578$, so the value of momentum peak p_{18} is higher than that of peak p_{19}, though the peak p_{19} is formed by absorbing four photons with a dominant frequency component. This analysis can also be used to understand momentum spectra in Figs. 4(b) and 4(c), where highest peaks are not formed by absorbing four photons with a dominant frequency component. By the way, when the modulation frequency at point C changes from $0.01m$ to $0.009m$, one can see that the number density is also increased, see Fig. 5(a), because the dominant frequency moves from $0.578m$ to $0.585m$; see Fig. 1(b).

In the range of $0.32 \leq \alpha \leq 1.0$, the minimum and maximum values of the number density of created pairs are E: 9.89×10^{-9} and F: 2.03×10^{-5}, respectively. It can be seen that the number density at point F is 200 times greater than that without frequency modulation ($N = 1.04 \times 10^{-7}$). It is noticeable that the value of α is 0.38 at point F, for which the effective frequency belongs to a reasonable area. Since the maximum effective modulation frequency should not be larger than the original laser frequency, the modulation parameters in the range of $\alpha \geq 1.0$ have no actual meanings and are not discussed anymore, although the number density of created particles is enhanced significantly in this region.

To explore the effect of the field strength and frequency on the enhancement of pair creation, we calculate the

pair number density varying with modulation parameters for a weak high-frequency field and a strong low-frequency field, respectively; see Figs. 5(b) and 5(c). From Fig. 5(b) and Table II, one can see that for the former case the maximum value of the number density of created pairs can reach H: 2.05×10^{-11}, which is 2000 times greater than the number density at point G where the field is not modulated. That is to say, the enhancement becomes more obvious for a weak high-frequency field. This is due to the fact that the n-photon thresholds (the peaks shown in Fig. 6) become more obvious for the weak high-frequency field and the frequency components play a key role in the enhancement of pair production. However, for a strong low-frequency electric field, see Fig. 5(c), the maximum value of the number density in a relatively reasonable area is J: 1.58×10^{-13}, which is only 8.82 times the number density for a field without modulation. This is because for the strong low-frequency field the pair production is dominated by the Schwinger tunneling mechanism and the frequency components have less effect on the pair creation. Therefore, a remarkable enhancement of pair creation corresponds to the frequency modulation of a weak high-frequency electric field. Furthermore, for a weaker high-frequency field the obvious enhancement still exists and the weak high-frequency field is expected in future experiments. For example, one of the two empty undulator tunnels in the European XFEL is proposed for the operation in ultrahard x-ray regime, up to the photon energy of 100 keV [35,36], and a gamma-ray laser based on a Bose-Einstein condensate of positronium was also put forward recently [37,38].

Based on the above discussion, we find that the number density of created pairs is not always enhanced by a frequency modulated field, but for certain modulation parameters it indeed can be increased significantly. Therefore, according to our theoretical analysis the particle number density may be enhanced by 2 or 3 orders of magnitude by conducting the most basic and precise modulation of a laser beam experimentally. It should be noted that the reason why the enhancement effect of pair production for the frequency modulated field here is much weaker than that for a linear chirped field is because the largest effective frequency of the frequency modulated field is restricted to less than two times the original frequency.

IV. CONCLUSION AND DISCUSSION

In summary, we investigate the momentum spectrum and number density of created electron-positron pairs in frequency modulated electric field and find that the momentum spectrum of created pairs shows an obvious interference pattern. This interference effect can be understood qualitatively by analyzing turning-point structures in the framework of the phase-integral method. It can also be explained more quantitatively by analyzing the frequency spectra of the frequency modulated field. It is found that the momentum peaks are determined by the pair creation process by absorbing photons with different frequencies. Moreover, we find that the number density of created pairs can be enhanced or weakened by adjusting the parameters of the frequency modulated field, but for certain modulation parameters it can be improved by 2 or 3 orders of magnitude. These results may provide a way to increase the number of created electron-positron pairs in future experiments.

It is well known that this type of modulated laser field we considered is usually used to transmit information in a communication system. In this paper, we find that the information carried by this field can also leave an imprint on the momentum spectrum of created pairs. Therefore, to some extent, we may obtain the information by analyzing the momentum spectrum. Furthermore, based on the recent work [28], where the electric field with temporally modulated amplitude can be manipulated in a controlled way to transmit information from a sender to a receiver by a new transport medium for information "Dirac vacuum", so it will be an interesting topic to check if the information carried by the frequency modulated electric field can be transmitted by the Dirac vacuum as well.

ACKNOWLEDGMENTS

C. G. would like to thank ILP for the nice hospitality during his visit to Illinois State University and acknowledges the China Scholarship Council program. The work of Z. L. L. and Y. J. L. is supported by the National Natural Science Foundation of China (NSFC) under Grants No. 11705278 and No. 11974419, in part by the National Key R&D Program of China under Grant No. 2018YFA0404802, and by the Fundamental Research Funds for the Central Universities. The work of B. S. X. is supported by the NSFC under Grants No. 11875007 and No. 11935008.

[1] P. A. M. Dirac, Proc. R. Soc. A **117**, 610 (1928).
[2] F. Sauter, Z. Phys. **69**, 742 (1931).
[3] J. S. Schwinger, Phys. Rev. **82**, 664 (1951).
[4] For a comprehensive review, see A. Di Piazza, C. Müller, K. Z. Hatsagortsyan, and C. H. Keitel, Rev. Mod. Phys. **84**, 1177 (2012).
[5] B. S. Xie, Z. L. Li, and S. Tang, Matter Radiat. Extremes **2**, 225 (2017).
[6] G. V. Dunne and C. Schubert, Phys. Rev. D **72**, 105004 (2005).
[7] G. V. Dunne, Q. H. Wang, H. Gies, and C. Schubert, Phys. Rev. D **73**, 065028 (2006).

[8] Q. Z. Lv, A. C. Su, M. Jiang, Y. J. Li, R. Grobe, and Q. Su, Phys. Rev. A **87**, 023416 (2013).
[9] M. Jiang, Q. Z. Lv, Z. M. Sheng, R. Grobe, and Q. Su, Phys. Rev. A **87**, 042503 (2013).
[10] Q. Su, W. Su, Z. Q. Lv, M. Jiang, X. Lu, Z. M. Sheng, and R. Grobe, Phys. Rev. Lett. **109**, 253202 (2012).
[11] C. Gong, Z. L. Li, and Y. J. Li, Phys. Rev. A **98**, 043424 (2018).
[12] S. P. Kim and D. N. Page, Phys. Rev. D **65**, 105002 (2002).
[13] S. P. Kim and D. N. Page, Phys. Rev. D **75**, 045013 (2007).
[14] E. Akkermans and G. V. Dunne, Phys. Rev. Lett. **108**, 030401 (2012).
[15] R. Alkofer, M. B. Hecht, C. D. Roberts, S. M. Schmidt, and D. V. Vinnik, Phys. Rev. Lett. **87**, 193902 (2001).
[16] F. Hebenstreit, R. Alkofer, and H. Gies, Phys. Rev. D **82**, 105026 (2010).
[17] Z. L. Li, D. Lu, B. S. Xie, L. B. Fu, J. Liu, and B. F. Shen, Phys. Rev. D **89**, 093011 (2014).
[18] Z. L. Li, D. Lu, B. S. Xie, B. F. Shen, L. B. Fu, and J. Liu, Europhys. Lett. **110**, 51001 (2015).
[19] Z. L. Li, Y. J. Li, and B. S. Xie, Phys. Rev. D **96**, 076010 (2017).
[20] G. R. Mocken, M. Ruf, C. Müller, and C. H. Keitel, Phys. Rev. A **81**, 022122 (2010).
[21] I. Akal, S. Villalba-Chávez, and C. Müller, Phys. Rev. D **90**, 113004 (2014).
[22] R. Schutzhold, H. Gies, and G. V. Dunne, Phys. Rev. Lett. **101**, 130404 (2008).
[23] A. Nuriman, B. S. Xie, Z. L. Li, and D. Sayipjamal, Phys. Lett. B **717**, 465 (2012).
[24] C. K. Dumlu, Phys. Rev. D **82**, 045007 (2010).
[25] M. Jiang, B. S. Xie, H. B. Sang, and Z. L. Li, Chin. Phys. B **22**, 100307 (2013).
[26] N. Abdukerim, Z. L. Li, and B. S. Xie, Chin. Phys. B **26**, 020301 (2017).
[27] O. Olugh, Z. L. Li, B. S. Xie, and R. Alkofer, Phys. Rev. D **99**, 036003 (2019).
[28] Q. Su and R. Grobe, Phys. Rev. Lett. **122**, 023603 (2019).
[29] D. Lawrence, *Frequency Modulation (FM) Tutorial* (Silicon Laboratories, Austin, 2008).
[30] C. K. Dumlu and G. V. Dunne, Phys. Rev. Lett. **104**, 250402 (2010).
[31] C. K. Dumlu and G. V. Dunne, Phys. Rev. D **83**, 065028 (2011).
[32] C. Schneider, G. Torgrimsson, and R. Schützhold, Phys. Rev. D **98**, 085009 (2018).
[33] E. Brezin and C. Itzykson, Phys. Rev. D **2**, 1191 (1970).
[34] C. Kohlfürst, H. Gies, and R. Alkofer, Phys. Rev. Lett. **112**, 050402 (2014).
[35] E. Schneidmiller, V. Balandin, W. Decking, M. Dohlus, G. Geloni, N. Golubeva *et al.*, in *Proc. FEL'19, Hamburg, Germany* (JACoW Publishing, Geneva, Switzerland, 2019), pp. 172–175.
[36] S. Serkez, C. Boffo, S. Casalbuoni, M. Dohlus, G. Geloni, S. Karabekyan *et al.*, in *Proc. FEL'19, Hamburg, Germany* (JACoW Publishing, Geneva, Switzerland, 2019), pp. 191–194.
[37] H. K. Avetissian, A. K. Avetissian, and G. F. Mkrtchian, Phys. Rev. Lett. **113**, 023904 (2014).
[38] H. K. Avetissian, A. K. Avetissian, and G. F. Mkrtchian, Phys. Rev. A **92**, 023820 (2015).